Advanced Steel Construction – Vol. 22 No. 3 (2026) 298–306
DOI:10.18057/IJASC.2026.22.3.5

THEORETICAL FEASIBILITY STUDY OF THE NEW STEEL GRATING WEB COMPOSITE BEAM

Jun Hu *, Yong-Yong Liang, Xin-Qi Zhang, Fu-Ming Yang and Liang-Jian Lai

School of Civil Engineering, Chongqing Jiaotong University, Chongqing, 400074, China

** (Corresponding author: E-mail: hujun@cqjtu.edu.cn)*

ABSTRACT

To reduce the self-weight and the steel consumption of the traditional steel-concrete composite beam, a new steel grating web composite (SGWC) beam is proposed by introducing a steel grating instead of the solid steel beam web. The uniaxial behavior, mechanical performance, load-displacement curve, and failure mechanism of the SGWC beam were studied, and the influence of steel grating size on their bearing capacity was thoroughly investigated. The results indicate that a 21.5% weight reduction in the SGWC beam versus traditional steel beams, and the strength, stiffness, and stability meet the requirements of the Chinese specification. In the elastoplastic analysis, the failure process of the SGWC beam can be divided into the elastic stage, the elastoplastic stage, and the plastic stage. The SGWC beam's load-bearing capacity reduces as grating spacing grows, but improves with greater grating thickness and width.

ARTICLE HISTORY

Received: 1 April 2025
Revised: 4 September 2025
Accepted: 20 September 2025

KEYWORDS

Composite beam;
Steel grating web;
Feasibility study;
Load-displacement curve;
Failure mechanism

1. Introduction

Bridges play a vital role in transportation as an infrastructure that crosses valleys and rivers and connects the transport between the two places [1, 2]. The steel-concrete composite beam comprises a concrete slab and a steel beam, which are connected by connectors and are stressed together. When used as a flexural member, these composite beams optimally combine concrete's compressive strength with steel's tensile capacity while avoiding the cracking and stability issues of pure RC or steel beams. Therefore, steel-concrete composite beams have become prevalent in bridge applications [3-5].

In recent years, as the span of bridge structures has increased, the dead weight and steel consumption of traditional steel-concrete composite I-beams have significantly risen. This not only results in higher material costs but also imposes more stringent requirements on the substructure and foundation. To address this challenge, scholars have proposed various technical solutions to enhance the bearing capacity of steel-concrete composite beams while reducing the structural weight. These solutions focus on enhancing concrete slabs, connectors, and steel webs.

Enhancing the performance of concrete slabs can significantly improve the application of steel-concrete composite beams. Men et al. [6] investigated the mechanical behavior of composite beams with UHPC-normal concrete composite slabs under negative bending moments and found that their application to composite beams can greatly enhance crack resistance while preserving bending capacity. Zha et al. [7] added UHPC to the traditional concrete bridge deck to form a composite bridge deck, and carried out several sets of tests to compare the bending properties of the composite beams. The results demonstrate the novel composite deck enhances beam performance by 13%. Jiang et al. [8] developed a prefabricated UHPC-steel pipe composite beam. The test shows that the composite beam has excellent bending performance and material utilization. Guo et al. [9] enhanced the structural bearing capacity and durability of steel-concrete composite beams by incorporating fiber-reinforced polymer reinforcement into the concrete slab.

As a critical component linking steel beams and concrete slabs, the arrangement of connectors significantly influences the bearing capacity of composite beams. Ding et al. [10] presents an angular connector that enhances the stiffness and anti-slip characteristics of composite beams. Luo et al. [11] developed innovative demountable bolted shear connectors, enhancing prefabricated composite beam performance through roll-out testing. Tzouka et al. [12] established a 3D numerical model to analyze novel shear connector behavior. This connector allows the bridge to be dismantled and can help to replace the aging bridge components, and the experimental results verify the reliability of the proposed model. Yang et al. [13] introduced a steel-concrete composite beam without a top steel flange and examined the application of various shear connectors within this structure. The results demonstrate that all connectors ensure the overall performance of the structure.

In traditional I-beams, the typical bending failure mode involves the simultaneous crushing of the concrete bridge deck and yielding of the bottom steel beam flange [14]. Structural efficiency is constrained by the weight of the solid steel beam, while the web's contribution to the structure's bearing capacity is also limited. Therefore, enhancing the web design is crucial for optimizing composite beam performance. The corrugated steel web is an effective design choice. To improve the cracking problem of composite beams, Pei et al. [15] replaced the flat steel web with corrugated steel webs, and carried out model tests to study the effect of web form on the bending and crack resistance of composite I-beams. Test results demonstrate the corrugated web design's superior crack resistance in bridge applications. Wu et al. [16] further demonstrated that corrugated steel webs are more advantageous in composite beams with spans exceeding 30 m. Honeycomb beam structures are widely used in civil construction in European and American countries due to their cost-effectiveness and efficiency [17]. Zhao et al. [18] compared the static loading test of the partially clad steel-concrete composite structure and the partially covered honeycomb steel-concrete composite beam to investigate the influence of the beam by the opening of the main steel web. In the case of similar materials, the honeycomb main steel web can improve the beam's bearing capacity compared with the traditional solid steel web by increasing the cross-sectional height through the appropriate opening. Still, it also reduces the material deformation capacity and is more affected by shear force.

Nowadays, with the development of bridge construction in mountainous areas, the steel-concrete composite beams with low requirements for hoisting equipment compared with other beams are a vital direction for bridge designers, and a key research challenge is to improve the engineering economy effectively of these composite beams [19]. As a material with a broad market prospect, steel grating plate has the advantages of high bearing performance and outstanding slip resistance under the same consumables and have been successfully applied to practical engineering [20-25]. Introducing this structure can significantly reduce the large amounts of steel used in I-beams.

Based on the above understanding, this study introduces a novel steel grating web composite (SGWC) beam that replaces the solid steel beam web with a steel grating plate based on the existing steel-concrete composite beam theory and design specifications. Taking the 60m simply-supported SGWC beam as the research object, the reasonable structure size, mechanical performance, and failure mechanism were studied. This research advances sustainable construction through improved composite beams structural performance suitable for prefabricated bridge applications.

2. The proposal of the SGWC beam

Steel gratings play an important role in areas such as tunnel supports, pedestrian bridges, and road paving, and are mostly arranged horizontally to withstand surface loads. Traditional steel-concrete composite beams often fail due to shear along the web at an oblique angle of 45°. Furthermore, referring to steel truss belly composite beam design, the optimal inclination angles for trusses with and without vertical rods are approximately 50° and 60°, respectively. Therefore, in this study, steel grating is oriented at a 45° angle to effectively resist shear forces, as illustrated in Fig. 1. The load-bearing mechanism is as follows: the oblique steel grating coincides with the main stress direction of the web and bears tensile stress and compressive stress, respectively, to provide strong shear bearing capacity for the composite beam by using the structure characteristics of the steel grating. Vertically arranged steel rods can transmit the vertical forces from the bridge deck and ensure stability.

Based on the above theory, this paper replaces the solid steel beam web with a steel grating for the composite beam. The steel beam of different webs is shown in Fig. 2.

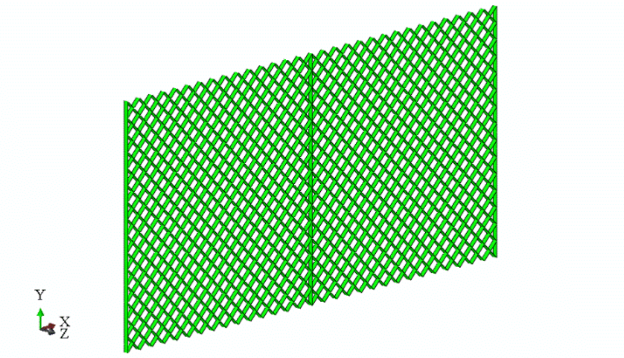

Fig. 1 Schematic diagram of the steel grating web

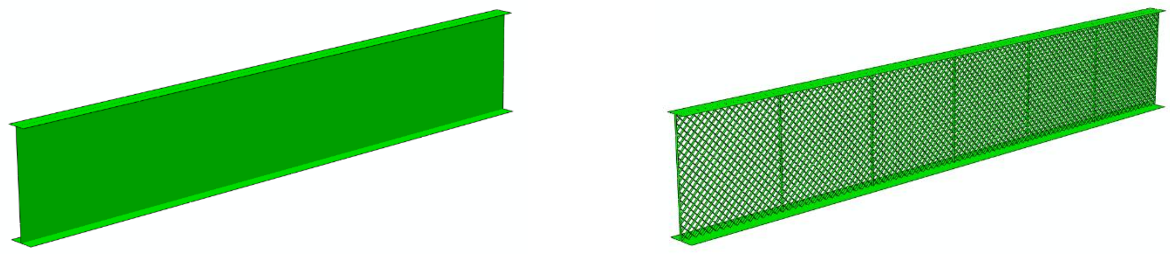

(a) The solid steel beam (b) The steel grating steel beam

Fig. 2 Schematic diagram of different web steel beams

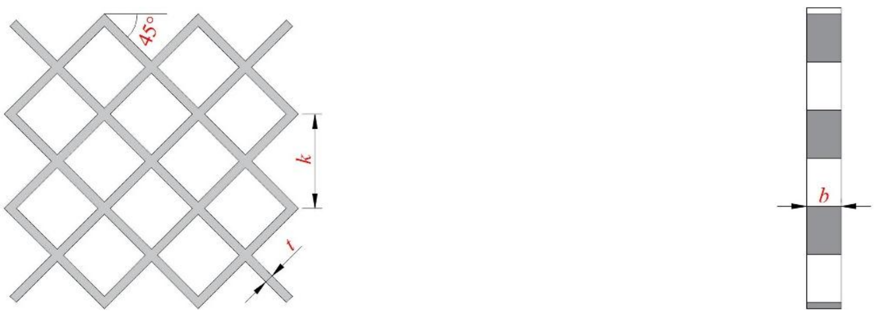

(a) Front view (b) Side view

Fig. 3 Schematic diagram of the steel grating

Fig. 3 illustrates the steel grating schematic, where *t* is the steel grating thickness, *k* is the steel grating spacing, the angle between the steel grating and the flange steel plates of the steel beam is 45 °, and *b* is the steel grating width.

For the steel grating web, its sizes should meet the width-to-thickness ratio and slenderness ratio requirements in the Chinese standard [26]. Referring to the Chinese specification [27], the common sizes of the steel grating are modified, and the specific size range is proposed in Table 1.

Table 1
Size parameters of the steel grating (mm)

t	*b*	*k*
5-35	30-120	Meets slenderness ratio and *b*/*t* limits

Table 2
The sizes of each composite beam (unit: mm)

	Traditional composite beams		The SGWC beam	
Span *l*	60000			
Beam height	3300			
Concrete slab	Width: 4250; Thickness: 250			
Upper flange steel plate	Width: 600; Thickness: 30			
Lower flange steel plate	Width: 800; Thickness: 45			
Web	Height: 2925	Thickness: 30	Height: 2925	*t*=30, *b*=50, *k*=200

According to the general design diagram of the 60m composite beam, the solid steel beam web is replaced by the steel grating and the other parameters are unchanged. The structure comprises concrete slabs, flange steel plates, and steel grating. According to the size parameter range of the steel grating proposed above, for the 60m SGWC beam, the specific sizes of each component are presented in Table 2, and the sizes of the traditional composite beams are also given.

Table 3 shows the comparison of the steel consumption of different composite beams with 60m spans. It can be seen from the table that the SGWC beam reduces web weight by 34.72% versus solid webs and cuts total steel weight by 21.5% compared to traditional beams, offering clear economic advantages.

Table 3
Comparison of the steel consumption in the two composite beams

Type	Traditional composite beams/m^3	The SGWC beam/m^3	Proportion of steel used /%
Web	5.27	3.44	65.28
Steel beam	8.51	6.68	78.50

Note: The proportion of steel used is the ratio of the steel consumption of the SGWC beam to the steel consumption of the traditional composite beam

In summary, a composite beam structure using steel grating instead of the solid steel beam web is proposed in this paper. Its overall load-bearing mechanism is as follows: the concrete slab and the upper flange steel plate bear the compressive stress, the lower flange steel plate bears the tensile stress, the oblique steel grating bears the shear stress, and the vertical steel grating is used to transmit the vertical force of the upper flange steel plate. When the SGWC beam is subjected to vertical load, the load is transferred from the concrete slab to the upper flange steel plate, and then to the lower flange steel plate through the steel grating web. In contrast to the shear stress generated by the web of traditional composite beams, the stress in the steel grating web of the SGWC beam is primarily dominated by axial force.

Compared with the existing composite beams [15-18], the SGWC beam can maximize the shear force-bearing capacity of the web, and it is convenient for replacing local components. Additionally, its unique mesh structure facilitates the dissipation of impact loads, reducing bridge vibration and enhancing driving stability. These findings demonstrate that SGWC beams offer strong stress performance while reducing the structure's weight and steel consumption, making them highly applicable.

3. Uniaxial behavior and method verification

The bearing capacity failure tests from literature are simulated via finite element analysis to quantify steel grating's fundamental tensile and compressive properties [28]. The experimental model is vertically arranged with 9 pieces of flat steel, the thickness of the flat steel arranged on both sides is 10 mm, and the thickness of 7 pieces of flat steel arranged in the middle is 8 mm. The width and spacing are both 120 mm, and the length of the flat steel is 3530 mm. Fig. 4 presents both experiment and corresponding finite element model.

(a) Experimental model (b) Finite element model

Fig. 4 Schematic diagram of steel grating

In the literature experiment, the vertical load is applied by using a jack at the top of the steel grating, and the displacement of the steel grating is controlled by arranging fasteners at the bottom. The analysis utilizes ABAQUS with S4R elements modeling flat steel and C3D8R elements discretizing frame members. The flat steel and the frame are bound constraints, and a common node is set between the flat steel and the steel bar to simulate the constraint effect. Vertical loads are applied through a reference point coupled to the member's top surface. The loading mode of displacement control is adopted, and the bottom of the component adopts the constraint mode of consolidation. The displacement nephograms in different directions of the steel grating members when they fail are shown in Fig. 5.

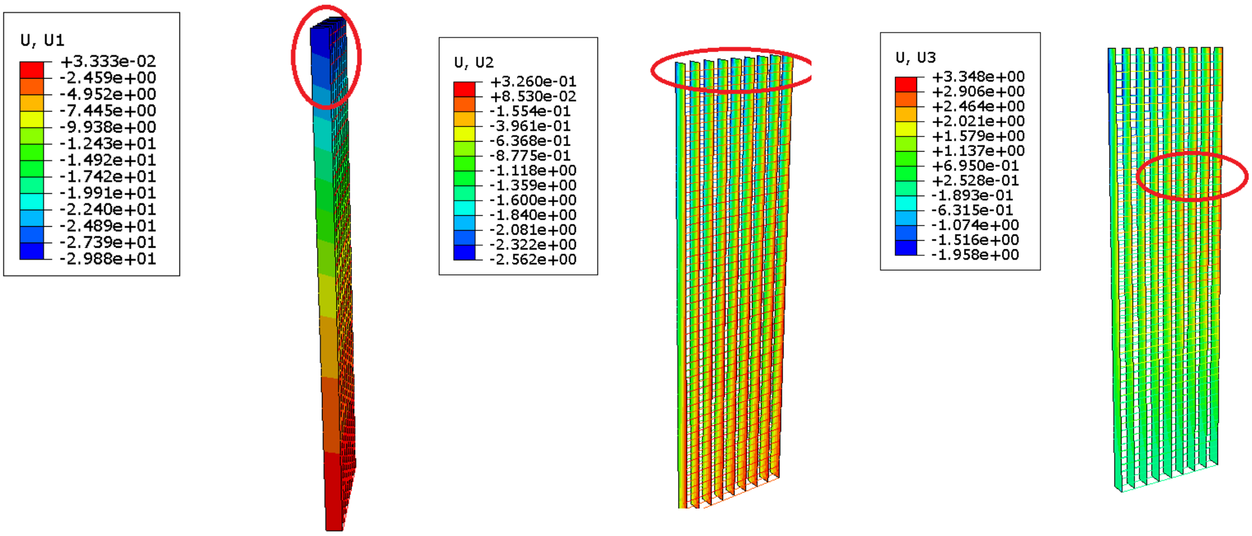

(a) Out-of-plane deformation (b) Vertical deformation (c) In-plane deformation

Fig. 5 Deformation nephograms of steel grating (unit: mm)

Table 4
Comparison of uniaxial behavior

Type	Bearing Capacity (kN)	Maximum displacement out of plane (mm)	Maximum displacement in plane (mm)	Maximum vertical displacement (mm)
Experiment	1435.8	-32.99	2.34	2.39
FEA	1369.4	-29.88	3.34	2.56

Table 4 compares experimental displacements from literature with present simulation results. It can be seen from the table that, except that the displacement of the steel grating member outside the plane is quite different from the calculation results in this paper, close agreement between simulation and experimental results validates the numerical model's accuracy.

Fig. 6 compares experimental and simulated load-displacement curve. As can be seen from the figure, the load displacement curve simulated by finite element analysis in this paper is approximately in a line rising state, indicating that the steel grating has a good linear elastic stage under uniaxial behavior. Moreover, the load displacement curve is very close to that obtained by the experiment, which once again verifies the accuracy of the work in this paper.

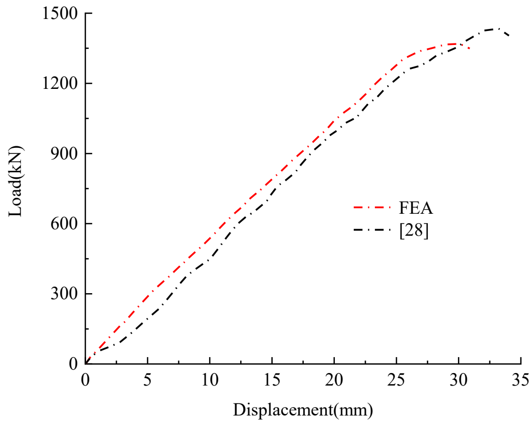

Fig. 6 Load displacement curve of steel grating under uniaxial behavior

4. Finite element analysis of the SGWC beam

In the finite element analysis, the steel is made of Q345, and the concrete slab is made of C50. The concrete slab is modeled with solid elements, and the flange steel plates and steel grating is modeled with shell elements. The concrete slab, flange plate, and steel grating are rigidly connected, which effectively avoids the difficulty of finite element analysis convergence and reduces the time of nonlinear iteration. When beam end constraints are applied to a finite element model, the fixed hinge bearing constrains the *x*, *y* and *z* axis, and the sliding hinge bearing constrains the displacement *x*-axis and *y*-axis.

Fig. 7 shows the finite element model of the 60 m SGWC beam. The entire beam is divided into 52,972 elements, with 46,131 nodes in total. There are four element sizes for the concrete slabs, with sizes in the *x*, *y*, and *z* directions as follows: $1\times0.1825\times0.125$ m^3, $1\times0.12\times0.125$ m^3, $0.2\times0.1825\times0.125$ m^3, and $0.2\times0.12\times0.125$ m^3. The upper flange steel plate consists of two element sizes: 0.1×0.0675 m^2 and 0.1×0.03 m^2 in the *x* and *y* directions, respectively. The lower flange steel plates come in two sizes: 0.1×0.0925 m^2 and 0.1×0.03 m^2. The steel grating has an element size of 0.1414×0.03 m^2.

The elastic modulus of steel and concrete is 206 GPa and 34.5 GPa, shear modulus is 79.23 GPa and 14.38 GPa, the mass density is 7.85×10^{-5} N/mm^3 and 2.5×10^{-5} N/mm^3, the linear expansion coefficient is 12×10^{-6}/°C and 10×10^{-6}/°C, and the Poisson's ratio is 0.3 and 0.2, respectively.

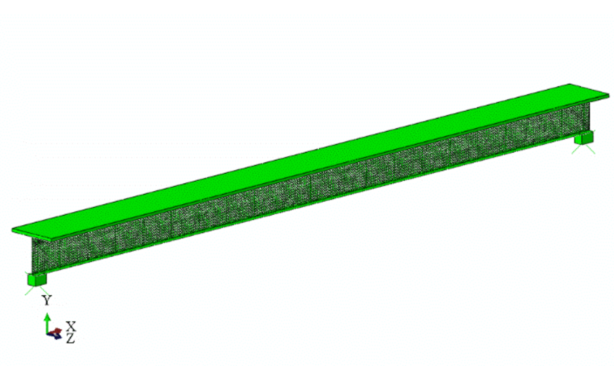

Fig. 7 Schematic diagram of the finite element model of the SGWC beam

4.1. Linear elastic analysis of the SGWC beam

In the strength checking of the SGWC beam, the basic combination of the ultimate limit states is used for loading according to the Chinese specification [29], and the partial safety factor for load is shown in Table 5.

Table 5
Partial safety factor for load

Self-weight	Second-phase load	Lane loads	Tempera-ture	Contraction creep	Wind load
1.2	1.2	1.4	1.05	1.0	1.1

The structural self-weight is automatically computed by the analysis software, and the temperature rise and drop are added through the temperature field in the finite element analysis. The second-phase load is 23.0 kN/m3 according to the weight of the asphalt concrete, and the thickness is 100 mm. In order to avoid the phenomenon of stress concentration, the 2 m concrete slab in the mid-span of the SGWC beam is coupled, and the concentrated load in the lane load is applied to the 2 m concrete slab. Fig. 8 presents the ultimate limit state longitudinal stress distribution across all beam components. Since the longitudinal stresses are symmetrically distributed along the mid-span, the left half of the beam was selected for the study, and the dimensions of the beam along the axis were reduced by half.

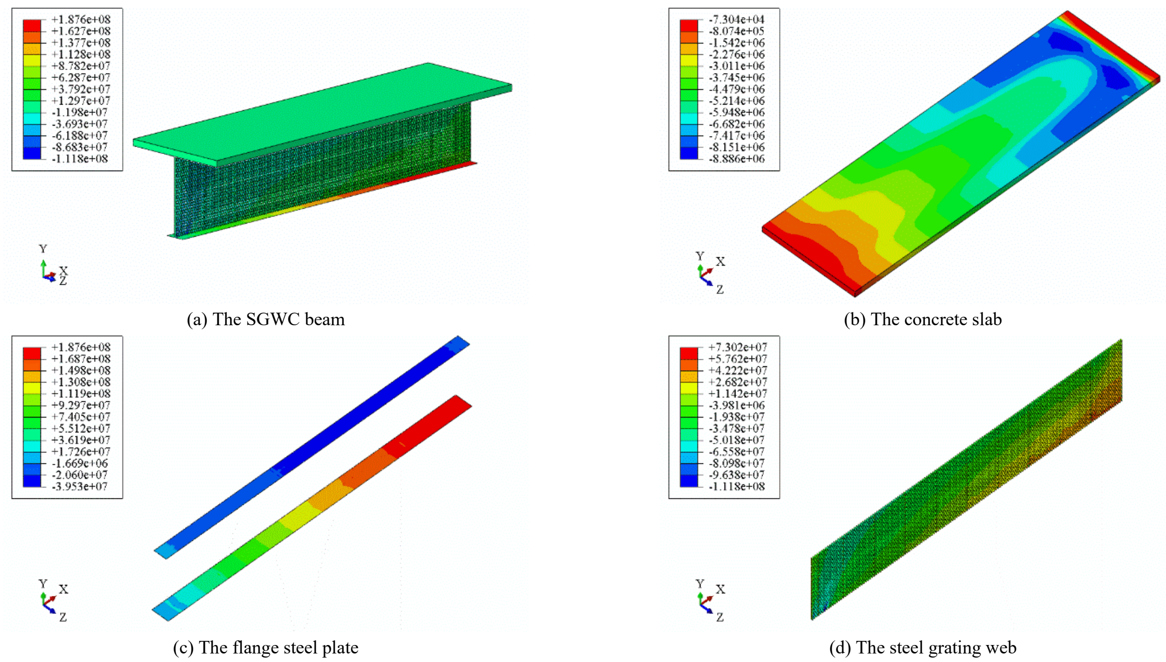

Fig. 8 Stress nephogram of the SGWC beam (unit: Pa)

Fig. 8 shows that the longitudinal stress of the concrete slab is gradually increasing from the bearing to the mid-span. Due to the influence of the way the concentrated load is applied, the maximum compressive stress occurs near the mid-span and its value is 8.89 MPa. Consistent with the concrete slab, flange plate stresses grow gradually toward mid-span while the upper flange remains in compression. The mid-span vicinity reaches maximum compressive stress of 39.53 MPa. The maximum value of the lower flange steel plate is 187.6 MPa in the middle section. The steel grating develops tensile stresses near mid-span while remaining regions sustain compression. The peak tensile stress occurs in the mid-span section, and its value is 73.02 MPa. Due to the arrangement of bearing at the end of the beam, this position exhibits the steel grating's highest compressive stress: 111.8 MPa. The stress of each component of the SGWC beam is less than the ultimate strength of the material, which meets the requirements of the Chinese specification.

When the stiffness of the SGWC beam is checked, 1.45 is selected as the long-term deflection growth coefficient according to the Chinese specification

[29]. The deflection is calculated according to the frequent combinations in the serviceability limit states. The calculation result is shown in Fig. 9. The figure shows that the maximum deflection of the SGWC beam is 47.2 mm. After considering the long-term increase coefficient, the deflection is 68.44 mm, which is smaller than the deflection limit l/550 (109 mm) specified in the Chinese specification [30], indicating that the stiffness of the SGWC beam meets the specification requirements.

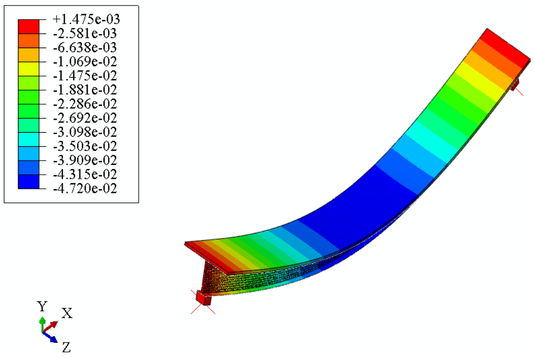

Fig. 9 The deflection of the SGWC beam (unit: m)

In the process of checking the stability of the SGWC beam, the stability coefficient of the first-order eigenvalue with practical significance can theoretically predict the structure's instability shape and ultimate load-bearing capacity. The second buckling mode is used in this paper. The instability shape and eigenvalue stability coefficient of the SGWC beam under the dead load and I-level lane load are calculated, as shown in Fig. 10. The figure shows that when the SGWC beam is destroyed, the first-order eigenvalue coefficient is 5.3438, while the stability safety factor is generally stipulated in the project is not less than 4. This indicates that the stability coefficient of the SGWC beam in the ideal linear elastic state not only meets the required standards but also exceeds the design value by 33.96%. This provides a sufficient safety margin and optimization potential for the stability coefficient of the SGWC beam, even after accounting for initial defects.

According to the results of the strength checking in the ultimate limit states, the stiffness checking in the serviceability limit states, and the stability checking, the structure of the SGWC beam is feasible and meets the specification requirements.

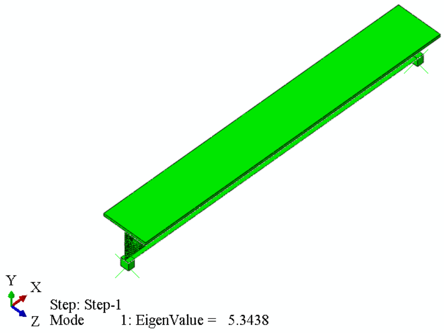

Fig. 10 Eigenvalue buckling mode of the SGWC beam

4.2. Elastoplastic analysis of the SGWC beam

A nonlinear finite element model accounting for material and geometric nonlinearity was developed for the SGWC beam. The constitutive relationship of the steel is given according to the Chinese specification [31], and the uniaxial stress-strain relationship is shown in Fig. 11. In the figure, *fy* is the representative value of the yield strength of the steel, fu is the representative value of the ultimate strength of the steel, *εy* is the yield strain of the steel, and *εu* is the peak strain of the steel. In this paper, the yield strength of the steel is 345 MPa, the tensile strength is 571 MPa, the elongation is 32%, and the cross-section shrinkage is 60%.

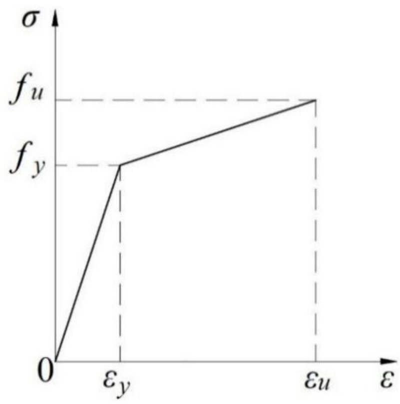

Fig. 11 Stress-strain curve of steel

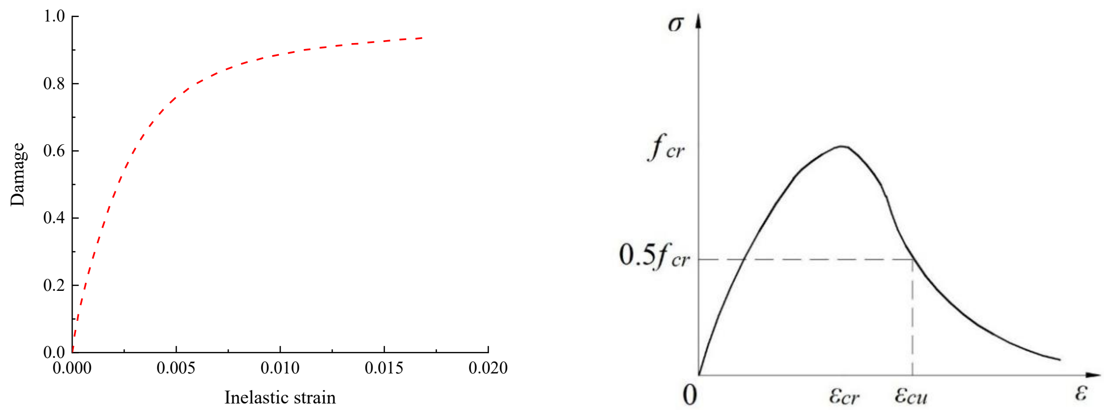

(a) Damage-inelastic strain curve (b) Compressive stress-strain curve

Fig. 12 Concrete elastoplastic model

In ABAUQS software, there are three types of concrete material models, and the concrete plastic damage model is selected for analysis. The damage-inelastic strain curve of concrete is shown in Fig. 12(a), in which the concrete adopts a damage factor that reflects the degradation rate of material stiffness. Concrete damage progresses from 0 (no damage) to 1 (total strength failure) in this quantification system. The constitutive relationship of concrete is given according to the Chinese specification [30], and the stress-strain relationship as shown in Fig. 12(b). In the figure, *fcr* is the representative value of the uniaxial compressive strength, *εcr* is the peak compressive strain, and *εcu* is the compressive strain when the stress is equal to 0.5*fcr*.

The applied load of the SGWC beam is the lane load, including the concentrated load applied in the mid-span and the uniform load in the full-span arrangement. Fig. 13 shows a schematic of the loading of the SGWC beam model with a span length l of 60 m.

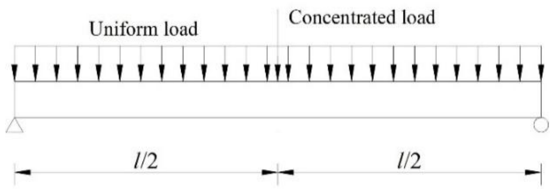

Fig. 13 Schematic diagram of model loading

Pu is defined as the ultimate bearing capacity, and *Pu* is determined according to the ultimate strength of the SGWC beam. ABAQUS simulated the complete load-to-failure behavior of the SGWC beam. Fig. 14 presents the load-displacement relationship of the SGWC beam under lane loading, derived from mid-span vertical displacement and bearing capacity data.

As can be seen from Fig. 14, the failure process of the SGWC beam consists of three stages: (1) the elastic stage with a load range of 0.0*Pu* -0.6*Pu*, and the load-displacement curve is basically in a linear rising state. At this stage, the elastic deformation of the SGWC beam occurs under the load, and the structure maintains an ideal elastic state. The steep load-displacement slope demonstrates high structural stiffness. (2) In the elastoplastic stage, the load range is 0.6*Pu* - 1.0*Pu*. In this stage, the concrete produces compressive damage, and the steel beam has plastic strain. The load-displacement curve shows a curve-rising state, and its slope gradually decreases, indicating that the stiffness of the SGWC beam gradually decreases; (3) During plastic deformation, concrete damage accumulates while the steel beam develops significant plastic strain, coinciding with peak load capacity. The load-displacement curve is horizontal, and the bearing capacity remains basically unchanged. The plastic deformation of the structure increases significantly until the SGWC beam fails, and the structure basically loses all its stiffness. On the whole, the failure form of the SGWC beam is flexural failure. The longitudinal stress of the SGWC beam at 1.0 *Pu* (ultimate bearing capacity) is shown in Fig. 15.

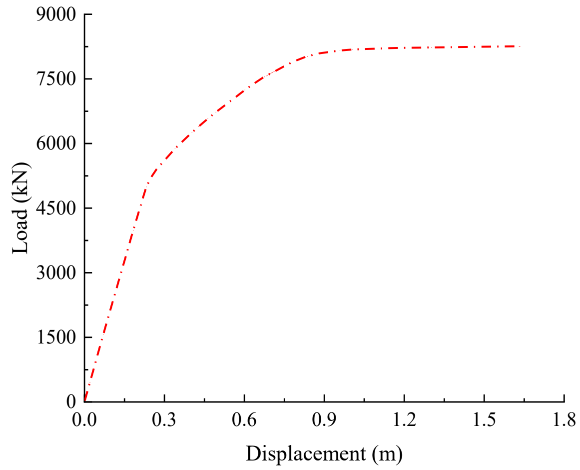

Fig. 14 Load-displacement curves of the SGWC beam

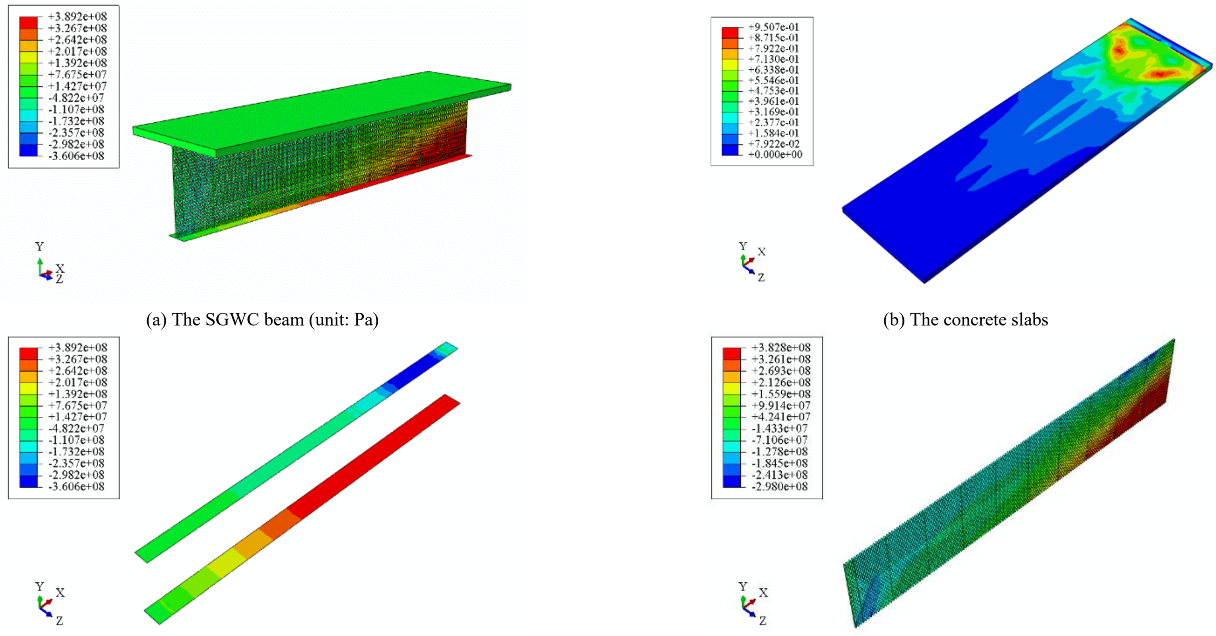

(a) The SGWC beam (unit: Pa) (b) The concrete slabs

(c) The flange plate (unit: Pa) (d) The steel grating (unit: Pa)

Fig. 15 Stress nephogram of each component of the SGWC beam at 1.0 *Pu*

It can be seen from Fig. 15 that when the SGWC beam achieves 1.0 *P*u, the concrete slab is compressed. The concrete damage gradually increased from the bearing to the mid-span, and the damage of the concrete slab near the mid-span was the most serious, with a damage factor of 0.95, but its distribution width was small. The flange plate stress also showed a gradual increase trend from the bearing to the mid-span, and the upper flange plate reached a peak compressive stress of 360.6 MPa. The maximum tensile stress of the lower flange plate is 389.2 MPa, which also occurs in the mid-span section. The stress of the steel grating is unevenly distributed along the longitudinal and vertical directions, and the maximum stress occurs in the mid-span, but the attenuation rate along the beam end is faster.

To further explore the stress distribution of the steel grating web, the steel grating near bearing, 1/4 span, and mid-span section of the SGWC beam was selected for analysis when the bearing capacity was 1.0 *P*u, and the stress distribution is shown in Fig. 16.

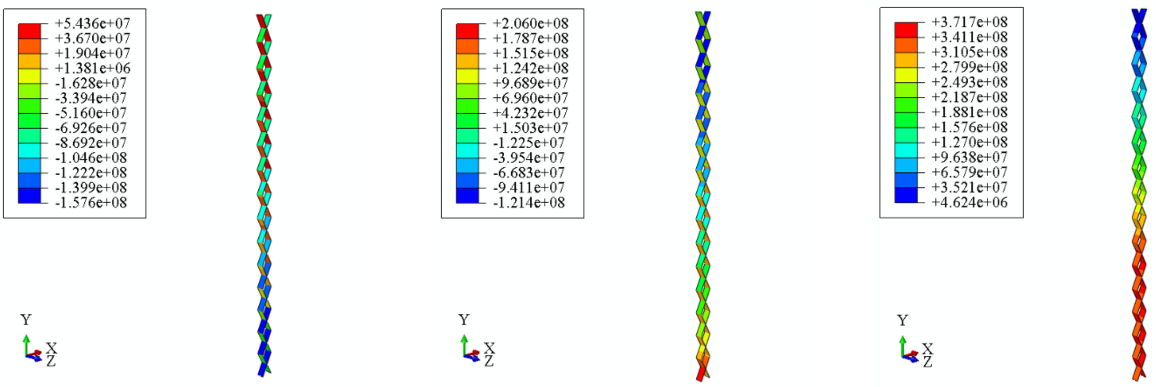

(a) Bearing (b) 1/4 span (c) Mid-span

Fig. 16 Stress nephogram of the steel grating with different cross-sections (unit: Pa)

Fig. 16 shows that the upper part of the steel grating near the bearing is in tension and the lower part is compressed. The peak stress of 157.6 MPa develops at the lower flange plate junction, and its upper stress is alternating between tension and compression. The stress distribution of the 1/4 span steel grating is compressed at the upper part and tensioned at the lower part. The maximum stress is tensile stress, which occurs at the junction with the lower flange plate and has a value of 206 MPa. The steel grating near the mid-span is all under tension, and its stress increases rapidly from top to bottom. The tensile stress is larger than that of the bearing and the 1/4 span cross-section, and the maximum value reaches 371.7 MPa.

From the stress distribution and maximum values of the steel grating, the steel grating's tensile stress exhibits gradual growth from the bearing toward mid-span, and the compressive stress near the lower flange plate at the bearing is the largest. The stress of the lower flange plate when the SGWC beam fails is shown in Fig. 17. Except for the contact part between the flange plate and the bearing under the SGWC beam, the rest of the flange plates are all under tension, and the maximum tensile stress in the mid-span is 389.2 MPa. The reason why the SGWC beam could not bear the load further was the destruction of the lower flange plate.

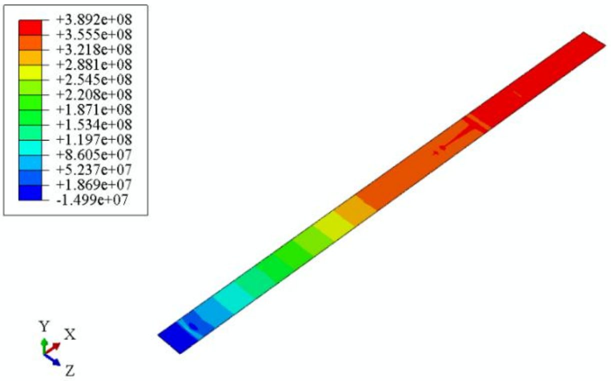

Fig. 17 The lower flange plate under failure of the SGWC beam (unit: Pa)

In summary, the results of elastic-plastic finite element analysis show that the SGWC beam exhibits flexural failure under the lane load. The lower flange plate is the most unfavorable position of the force, and it is the first to reach the ultimate strength and destruction, which leads to the decrease of SGWC beam's bearing capacity. In practical engineering applications, the overall performance of the SGWC beam can be enhanced by using high-strength steel for the lower flange plate, adding stiffeners in the middle span, and incorporating prestressing technology.

5. Parametric analysis

As shear failure must be prevented and the SGWC beam represents a novel structural form, current specifications lack applicable dimensional guidelines. To ensure the bending failure of the SGWC beam, finite element numerical simulation is used in this section to determine the size limit and the influence of size changes of the steel grating under the design size on the failure mode of the SGWC beam. This ensures safe SGWC beam applications and provides design criteria for future engineering practice.

(1) The steel grating spacing *k*

The steel grating spacing is 150 mm, 200 mm, 250 mm, 300 mm, and 375 mm, respectively, and the remaining parameters of the SGWC beam are kept unchanged. The load-displacement curve under different spacing is drawn as shown in Fig. 18. The figure shows that the bearing capacity of the SGWC beam declines as the steel grating spacing grows. The SGWC beam with a spacing of no more than 300 mm has a relatively obvious plastic deformation stage.

Table 6 presents the SGWC beam's bearing capacity, maximum flange plate and steel grating stresses, and concrete damage states across varying grating spacing. As can be seen from the table, when the steel grating spacing is 375 mm, the maximum stress of the SGWC beam occurs in the steel grating web. Combined with the load-displacement curve of Fig. 18, there is no obvious plastic deformation stage of the load-displacement curve under this spacing, and shear failure occurred in the SGWC beam. With the gradual decrease of the spacing, the maximum normal stress occurs in the flange plate, and the load-displacement curve has an obvious plastic deformation stage. It indicates that the spacing of the steel grating should not be greater than 300 mm.

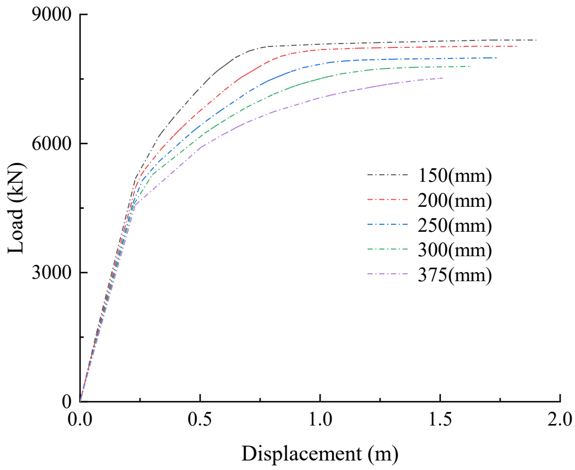

Fig. 18 Variation curve of load-displacement curve with the steel grating spacing

Table 6
Numerical simulation results under different steel grating spacing

k(mm)	*Pu*(kN)	σ_F (MPa)	σ_W (MPa)	Concrete damage
150	8404.95	397.4	389.9	0.96
200	8258.53	395.8	382.7	0.96
250	7991.34	391.8	387	0.96
300	7792.74	391	385.5	0.96
375	7520.39	377.7	-396.8	0.96

Note: σ_F and σ_W are the normal stress of the flange plate and steel grating, respectively.

(2) The steel grating thickness *t*

The steel grating thickness starts from 10 mm and increases in 5 mm steps to 30 mm, and the remaining parameters of the composite beam are kept unchanged. The load-displacement curve under different steel grating thicknesses is drawn, as shown in Fig. 19. The figure shows that the bearing capacity of the SGWC beam increases with the rise of the steel grating thickness, and the growth rate of the bearing capacity decreases greatly when the thickness exceeds 20 mm. The SGWC beam with a thickness of not less than 20 mm has a relatively obvious plastic deformation stage.

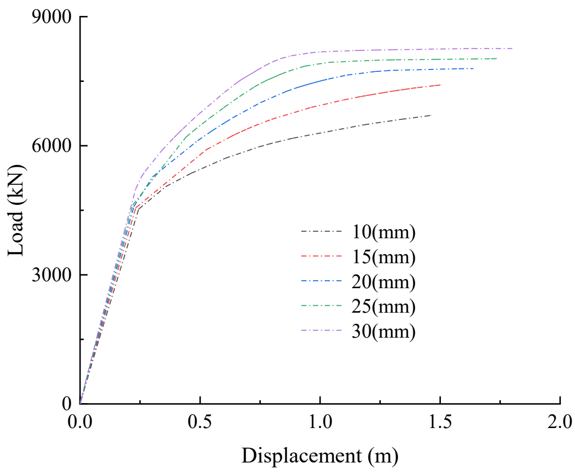

Fig. 19 Variation curve of the load-displacement curve with the steel grating thickness

Table 7 presents the SGWC beam's bearing capacity, maximum flange plate and steel grating stresses, and concrete damage states across varying grating thicknesses. As can be seen from the table, when the thickness is 10 mm, the steel grating web yields first, the flange plate and the concrete still have bearing capacity, and the SGWC beam undergoes shear failure. When the thickness is 15 mm, the flange steel plate experiences peak stress in the composite beam. However, combined with the load-displacement curve of Fig. 19, there is no obvious plastic deformation stage of the SGWC beam at this thickness. As the thickness increases, peak stresses concentrate in the flange steel plate. At this time, the concrete slab loses its bearing capacity, and the load-displacement curve has an obvious plastic deformation stage. It indicates that the thickness of the steel grating should not be less than 20 mm.

Table 7
Numerical simulation results under different steel grating thicknesses

t(mm)	Pu(kN)	σ_F (MPa)	σ_W (MPa)	Concrete damage
10	6704.56	359	-391.4	0.75
15	7413.98	394.3	384.9	0.88
20	7793.94	391.2	383.7	0.96
25	8024.78	392.2	383.5	0.96
30	8258.53	395.8	382.7	0.96

(3) The steel grating width b

The steel grating width starts from 20 mm and increases in 10 mm steps to 60 mm, and the remaining parameters of the composite beam are kept unchanged. The load-displacement curve under different steel grating widths is drawn, as shown in Fig. 20. The figure shows that the SGWC beam's bearing capacity rises with width, but growth slows significantly beyond 40 mm. The SGWC beam with a width of not less than 40 mm has a relatively obvious plastic deformation stage.

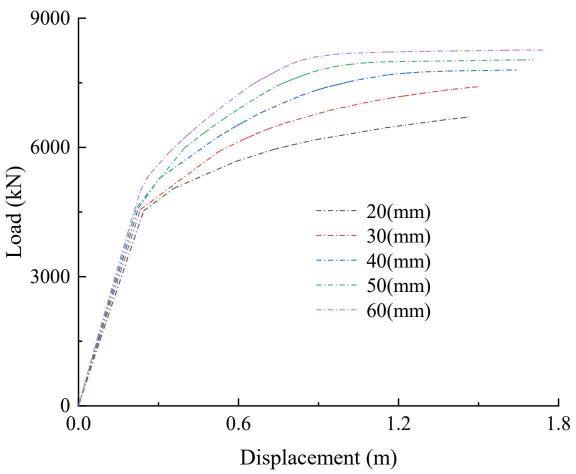

Fig. 20 Variation curve of the load-displacement curve with the steel grating width

Table 8 presents the SGWC beam's bearing capacity, maximum flange plate and steel grating stresses, and concrete damage states across varying grating widths. As can be seen from the table, when the width is 20 mm, the web of the steel grating is buckled, and the concrete and flange steel plates do not completely lose their bearing capacity, and the SGWC beam structure undergoes shear failure. When the width is 30 mm, the maximum normal stress of the composite beam occurs in the flange plate. The failure modes of the SGWC beam evolve with increasing width as follows: the flange plate yields first, the concrete is crushed, and the load-displacement curve has an obvious plastic deformation stage. It indicates that the width of the steel grating should not be less than 40 mm under the current design dimension.

Table 8
Numerical simulation results under different steel grating widths

b(mm)	Pu(kN)	σ_F (MPa)	σ_W (MPa)	Concrete damage
20	6703.82	370.5	-396.3	0.75
30	7414.34	390.7	385.9	0.88
40	7797.87	390.6	384.5	0.96
50	8034.03	394.3	383.9	0.96
60	8258.53	395.8	382.7	0.96

6. Discussions

This paper replaces the conventional composite beam web with a steel grating. The linear elastic mechanical properties of the beam are analyzed using the finite element method, followed by elastoplastic analysis to ensure plastic failure criteria are met. The research and development of the SGWC beam aim to address the disadvantages of traditional composite beams, including excessive dead weight and high steel consumption. However, the successful application of the SGWC beam depends on its compatibility with existing bridge construction standards and practices. This is critical for its integration into the current system and widespread use in practical projects.

6.1. Design standard compatibility

The design of the SGWC beam follows the current specifications for steel-concrete composite beams, and the material properties comply with the relevant standards. Linear elastic analysis results show that the SGWC beam complies with Chinese specifications in strength, stiffness, and stability, indicating its suitability for current standards under normal use conditions. Although the current research focuses on the basic stress performance, further analysis of wind-induced vibrations and seismic performance is required per relevant specifications to ensure the safety of the SGWC beam under extreme load conditions.

6.2. Construction compatibility

Existing construction methods, such as prefabricated assembly and cast-in-place, are suitable for the SGWC beams. Given the structural characteristics of the SGWC beam, the prefabricated assembly method offers certain advantages. Commonly used construction equipment in bridge construction is largely applicable. The reduced weight of the SGWC beam allows for optimized equipment selection based on its actual weight, with adjustments mainly needed for parameters like concrete pouring to match the structural characteristics. For specialized construction processes, such as on-site welding of steel grating plates, specialized welding equipment may be required, along with strict control of the welding process to meet quality standards.

6.3. Maintain management compatibility

Existing testing methods, including appearance testing, non-destructive testing, and load testing, are suitable for the SGWC beams, with the addition of key part detection of the steel grating plate. Bridge maintenance and repair can follow existing measures. Conventional measures, such as concrete crack repair and steel structure rust removal and painting, are effective. During maintenance, the special structure of the steel grating plate must be considered, with attention given to hole coating coverage and the inspection of connection parts.

In summary, the SGWC beam is compatible with existing bridge construction standards and practices. However, it requires design, construction, and maintenance optimization to accommodate its unique structural form, ensuring its safe application and long-term performance in engineering projects.

7. Conclusions

This paper proposes a new steel grating web composite beam. Its basic mechanical principle is analyzed, and the feasibility of the structure is checked. The bearing capacity is analyzed by studying its failure mechanism, and the following conclusions are obtained:

(1) The SGWC beam mainly comprises the concrete slab, the steel grating web, and the flange steel plates. The steel grating web is primarily used to bear the shear force, and the concrete slab and flange steel plates are used to bear the bending moment. Based on industry standards and specification requirements, the size range of the SGWC beam is formulated. In addition, in uniaxial behavior, the steel grating exhibits excellent linear elastic characteristics.

(2) The linear elasticity analysis for the 60 m simply-supported SGWC beam is adopted. Its strength, stiffness, and stability meet the specification requirements, and the structure's feasibility is verified. The self-weight can be reduced by 21.5% compared with the traditional steel beam under the current proposed size, and the engineering cost and assembly difficulty are effectively reduced.

(3) The failure mechanism of the SGWC beam was analyzed by elastoplastic finite element, and the failure process consists of three stages, namely the linear elastic stage (0.0 Pu -0.6 Pu), the elastoplastic stage (0.6 Pu - 1.0 Pu) and the plastic stage. In the whole process of failure, the stress of the lower flange plate first reaches the ultimate strength, resulting in the SGWC beam not being able to continue to bear the load.

(4) The load-bearing capacity of the SGWC beam decreases with the increase of the steel grating spacing and rises with the increase of the thickness and width of the steel grating. To ensure that the SGWC beam does not suffer shear failure under the design size of this paper, the spacing of the steel grating should not be greater than 300 mm, the thickness should not be less than 20 mm, and the width should not be less than 40 mm.

(5) This paper investigates the mechanical performance of the SGWC beam using numerical simulations and analyzes the uniaxial stress test of the proposed steel grating. However, the model test of the composite beam is crucial as it can significantly address the limitations of numerical analysis. Future research will focus on model trials of SGWC beams and their application in continuous beam bridges. Additionally, considering the shear resistance of the web, arranging the

steel grating with variable spacing can significantly optimize the web design. The study of the steel grating web wrapping the concrete to effectively inhibit its buckling and improve the overall bearing capacity will also be carried out.

Declaration of competing interest

The authors declare there are no competing interests.

Acknowledgment

This work was supported by the [Chongqing Joint Training Base for Postgraduate] under Grant [JDLHPYJD2020020].

Data availability statement

The data that support the findings of this study are available from the corresponding author upon reasonable request.

References

[1] Pelke, E. (2024) "Evaluation and strengthening of existing bridges- historical outlines and findings regarding the Hessian road bridge in-ventor". Bautechnik. 101(10): 568-581. DOI10.1002/bate.202400031
[2] Yan, J.B., Kang, E.C., and Xie, J. (2023) "Behaviors of steel-concrete composite beams at low temperatures: materials and structures". Advanced Steel Construction. 19(4):353-365. DOI: 10.18057/IJASC.2023.19.4.4
[3] Feng, B.W., Liu, Y.J., Yang, X., Liu, J., Zhang, G.J., and Ma, Y.P. (2023) "Experimental research on curved continuous steel-concrete composite twin I-girder bridge". Structures. 54:669-683. DOI: 10.1016/j.istruc.2023.05.081
[4] Ibrahim, T.H., Allawi, A.A., and El-Zohairy, A. (2023) "Experimental and FE analysis of composite RC beams with encased pultruded GFRP I-beam under static loads". Advances in structural engineering. 26(3): 516-532. DOI: 10.1177/13694332221130795
[5] Liu, J., Lyu, F., Ding, F.X., and Liu, X.M. (2022) "Energy dissipation of steel-concrete composite beams subjected to vertical cyclic loading". Advanced Steel Construction. 18(3):658-669. DOI: 10.18057/IJASC.2022.18.3.3
[6] Men, P, Chen, FM, Qin, FJ, Peng, X, Di, J, Jiao, HR. (2022) "Behavior of composite beams with UHPC-concrete composite slabs under negative bending moment". Journal of constructional steel research. 227:109415. DOI: 10.1016/j.jcsr.2025.109415
[7] Zha, S., Deng, W.Q., Liu, D., Zhang, J.D., and Gu, J.C. (2024) "Experimental study on flexural behavior of steel-laminated concrete (NC and UHPC) composite beams with corrugated steel webs". Engineering Structures. 306:117802. DOI: 10.1016/j.engstruct.2024.117802
[8] Jiang, J.L., Wang, H.J., Zhou, Z.X., Liang, H.P., Zhang, Z.Y., He, Z.S., and Zou, Y. (2025) "Flexural behavior of prefabricated steel-UHPC composite beams with hollow UHPC bridge deck". Journal of constructional steel research. 226:109267. DOI: 10.1016/j.jcsr.2024.109267
[9] Guo, Q., and Chen, H. (2024) "Bending analysis of recycled concrete beams reinforced with GFRP bars under high temperature". Advanced Steel Construction. 20(3):292-299. DOI: 10.18057/IJASC.2024.20.3.8
[10] Ding, K.W., Zhang, X.Q., Liu, Y.L., He, S.L., Wang, J.F., and Shen, W.Y. (2022) "Research on Angle Connector in Composite Beam". International journal of concrete structures and materials. 16(1):15. DOI: 10.1186/s40069-022-00507-x
[11] Luo, Y.B., Sun, S.K., Yan, J.B., Zhao, Y.C., and Lam, D. (2022) "Shear behavior of novel demountable bolted shear connector for prefabricated composite beam". Advanced Steel Construction. 18(4):745-752. DOI: 10.18057/IJASC.2022.18.4.2
[12] Tzouka, E., Karavasilis, T., Kashani, M.M., and Afshan, S. (2021) "Finite element modelling of push-out tests for novel locking nut shear connectors". Structures. 33:1020-1032. DOI: 10.1016/j.istruc.2021.04.088
[13] Yang, Y.L., Han, J.J., Zhao, Y., Yu, Y.Y., and Chen, Y.F. (2023) "Shear behavior of web-embedded steel-concrete composite beam". Advances in structural engineering. 26(5):842-857. DOI: 10.1177/13694332221097730
[14] Yan, J.B., Kang, E.C., Xie, J. (2024) "Behaviours of steel-concrete composite beams at low temperatures: materials and structures". Advanced Steel Construction. 19(4):353-365. DOI: 10.18057/IJASC.2023.19.4.4
[15] Pei, H.T., Zha, S., Wu, T.Y., Li, B.D., Zhan, G.Y., and Deng, W.Q. (2025) "Experimental study on flexural behaviour of prefabricated steel-concrete composite I-beams under negative bending moment: comparative study". Material. 18(2):450. DOI: 10.3390/ma18020450
[16] Wu, Y.F., Pan, W.H., and Luo, Y.Z. (2023) "Economical Design Comparison of Large-Span Composite Floor Systems with I Beams and Corrugated Web Beams". Buildings. 13(8):1940. DOI: 10.3390/buildings13081940
[17] Ferreira, F.P.V., Martins, C.H., and De Nardin, S. (2020) "Advances in composite beams with web openings and composite cellular beams". Journal of constructional steel research 172:106182. DOI: 10.1016/j.jcsr.2020.106182
[18] Zhao, B.D., Zhang, X.F., Wang, W., and Fu, L.F. (2023) "Experimental study on flexural behavior of partially-encased composite beam with castellated steel and concrete". Journal of Building Structures. 44:161-171. DOI: 10.14006/j.jzjgxb.2022.0172
[19] Nawar, M.T., El-Zohairy, A., Maaly, H.M., Husain, M., Salama, I., and Mousa, E. (2023) "Prestressed Steel-Concrete Composite I-Beams with Single and Double Corrugated Web". Buildings. 13(3):647. DOI: 10.3390/buildings13030647
[20] Liu, Y., Wu, H., Yu, Q., Li, Y., Li, J.N., and Li, L.Z. (2021) "Seismic performance of grille-type steel plate concrete composite walls with application in a super-high-rise building". Applied Sciences. 11:7580. DOI: 10.3390/app11167580
[21] Yu, Q., Wu, H., Li, L.Z., Ogail, E., Liu, Q.Y., Zhao, X.L., and Liu, Y. (2023) "Seismic performance analysis and evaluation of tall structures using grille-type steel plate composite shear walls". The Structural Design of Tall and Special Buildings. 32(13), e2037. DOI: 10.1002/tal.2037
[22] Ma, J.Y., Yuan, H.Y., Zhang, J.H., and Luo, Z.L. (2024) "Numerical and Theoretical Study on Flexural Performance and Reasonable Structural Parameters of New Steel Grating-UHPFRC Composite Bridge Deck in Negative Moment Zone". Buildings. 14(9):2857. DOI: 10.3390/buildings14092857
[23] Li, L., Wang, H.W., Wu, J., Li, S.T., and Wu, W.J. (2021) "Experimental investigation on dynamic tensile behaviors of engineered cementitious composites reinforced with steel grid and fibers". Materials. 14:7042. DOI: 10.3390/ma14227042
[24] Philip, R.B., Mohan, A., Akhila, B., Alexander, A., and Mathew, J. (2022) "Comparative study of conventional slab with slab constructed using AAC block and steel grid". Materials Today: Proceedings. 65:448-454. DOI: 10.1016/j.matpr.2022.02.634
[25] Abdulla, W., and Menzemer, C. (2021) "Finite element analysis of heavy duty riveted steel grating bridge deck". CivilEng. 2:485-501. DOI: 10.3390/civileng2020027
[26] China Architecture & Building Press, Beijing, China. (2017) Standard for design of steel structures (GB 50017-2017).
[27] Metallurgical Industry Press, Beijing, China. (2019) The People's Republic of China ferrous metallurgy industry standard (YB/T 4001.1-2019).
[28] Zhang, Z.W. (2005) Experimental study on the static and seismic behavior of steel grid bearing wall. Beijing University of Technology, Beijing, China.
[29] China Communication Press, Beijing, China. (2015) General specifications for design of highway bridges and culverts (JTG D60-2015).
[30] China Architecture & Building Press, Beijing, China. (2021) General code for composite structures (GB 55004-2021).
[31] China Architecture & Building Press, Beijing, China. (2010) Code for design of concrete structures (GB 50010-2010).